

THE IMAGE-SOURCE REVERBERATION MODEL IN AN N-DIMENSIONAL SPACE

Stephen McGovern

Spacenet, Inc.

McLean, VA, United States

smcgover@alumni.stevens.edu

ABSTRACT

The image method is generalized to geometries with an arbitrary number of spatial dimensions. n -dimensional (n -D) acoustics is discussed, and an algorithm for n -D room impulse response calculations is presented. Synthesized room impulse responses (RIRs) from n -D rooms are presented. RIR characteristics are discussed, and computational considerations are examined.

1. INTRODUCTION

Reverberation is a widely used and indispensable audio effect. It is used to simulate environmental acoustics and as a means for artistic modification of audio.

Descriptions of reverberation are often broken into two portions, the early echoes and the tail. The characteristics of each portion is important for predicting the resultant effect [1] [2] [3]. Early echoes are important for conveying spatial information to the listener. This is often implemented in commercial reverberators as a tunable parameter referred to as "pre-delay." The tail portion of the reverberation response can vary greatly in length and thereby determines how long reverberation persists after an excitatory input.

Before digital electronics became commonplace, room acoustic simulation was achieved through analog means. Audio signals were processed mechanically by transmitting vibrations through a spring or a plate. Today, digital emulations of springs and plates are popular with musicians and they continue to be the topic of many papers such as [4] [5] and [6] [7], respectively.

Comb and all-pass filters have long been used in reverberators. The approach can be generalized as a feedback delay network (FDN) [8] and it has the benefit of having relatively low computational overhead [9].

Various wave-based models have been a popular research topic. They have the drawback of being computationally intensive, although progress is being made to accelerate computation [10].

It is also possible to measure an RIR using a real room. This may be done either for analysis or as an finite impulse response (FIR) filter for direct simulation. Implementation of FIR filters tend to require greater overhead than FDNs; however, this is now less of an issue as computers have become more powerful. Methods such as segmented convolution can be used to reduce latency [9].

RIRs can also be synthesized using methods based in geometrical acoustics theory. Methods using this approach include mirror images [11], ray tracing [12], and, more recently, beam tracing [13]. Aside from the typical time domain models, frequency domain methods exist as well [14] [15]. The validity of these types of simulations was explored in [16].

While geometrically complex rooms have been simulated, the additional physical complexity requires higher algorithmic complexity. Models of box-shaped rooms, however, are sufficient for many purposes and they continue to be an active topic in research [9] [11] [14] [15].

There are other effects related to reverberation, though some might not clearly meet the criteria for what is commonly understood to be reverberation. These include delay, gated reverb, musical instrument body models [17] [18], and resonance effects [19]. While this paper will not deal with such concepts directly, it has been written in the context of the full scope of reverberation-related effects.

1.1. Review of Dimensionality in Existing Models

There has been very little research in the area of n -dimensional reverberation. There are, however, a few notable exceptions [20] [21] [22]. These papers discussed n -D DWM, hyperdimensional finite difference time domain (FDTD) mesh, and hyperdimensional DWM, respectively.

In contrast, most reverberation algorithms are either developed in reference to some type of 3-D acoustic space or they seek to directly model a 3-D acoustic space. Examples of this include wave-based methods [10], the image method [23], and beam tracing [13].

Aside from 3-D models, equivalent 2-D models have been studied as well. Two dimensional digital waveguide mesh (DWM) implementations have been used to model both 2-D acoustic spaces [24] [25] and vibrations on plates and membranes [26]. A 2-D image method has been used to model room reverberation [27], and a 2-D beam tracer has been used to model acoustics in [28] [29].

Outside of the field of room simulation, the image method has been used to model vibration in 1-D beams [30], 1-D beams and 2-D plates [31], and 2-D plates [32]. While there is little published discussion of reverberation models based on 1-D systems, such models produce delay effects. Interestingly enough, delay and reverberation are easily confused by novice musicians.

What is lacking in all of this is a unified model characterizing 1-D, 2-D, and 3-D systems using a method based on geometrical wave theory. There is also no such model comparable to the mesh simulations described in [21] [22] that is extendable to higher dimensions. There is very little formal discussion on why 1-D, 2-D, and 3-D models all produce similar effects, and there is a void of research regarding how higher dimensional resonant systems ought to sound.

Sec. 2 discusses background mathematics related to RIR calculations. Sec. 3 examines n -D geometry and its implications for rooms and acoustics. Algorithmic implementation is discussed in Sec. 4. In Sec. 5, implications of n -D room simulations are

analyzed. An approach for modeling non-integer dimensions is presented in Sec. 6. Sec. 7 examines algorithmic efficiency, presents benchmarks, and then discusses simulations. Finally, Sec. 8 presents the conclusions.

2. BACKGROUND MATHEMATICS

The image method generates an impulse response by creating mirror images of a sound source across the walls of an enclosure. The acoustical pressure impulse of the image with index q is given by

$$p(r, t)_q = \frac{A_q}{|\mathbf{r} - \mathbf{r}_q|} \delta \left(t - \frac{|\mathbf{r} - \mathbf{r}_q|}{c} \right) \quad (1)$$

where A_q is a constant, $|\mathbf{r} - \mathbf{r}_q|$ is the distance between the receiver and the q th source, δ is the Dirac delta function, and c is the speed of sound. The pressure impulses are then summed together as if they are a superposition of independent sources. This results in the pressure impulse response function given by

$$h(t) = \sum_q p(t)_q \quad (2)$$

where the summation takes place over all images in 3-D.

By taking the Fourier transform of Eq. 1 the acoustical pressure impulse may be given in the frequency domain as

$$p(w, t)_q = \frac{A_q}{|\mathbf{r} - \mathbf{r}_q|} e^{-j \frac{w}{c} |\mathbf{r} - \mathbf{r}_q|} \quad (3)$$

This results because of a property of the Dirac delta function. This property was given in [33]. In a fashion similar to Eq. 2, the summation may be taken in the frequency domain. This results in

$$H(\omega) = \sum_q p(w, t)_q \quad (4)$$

In [34] it was shown that the inverse Fourier transform of Eq. 4 could be taken to yield an expression equivalent to Eq. 2.

$$h(t) = \frac{1}{2\pi} \int_{-\infty}^{\infty} H(\omega) e^{j\omega t} d\omega \quad (5)$$

n -D box-shaped enclosures can preserve much of the simplicity of 3-D box-shaped enclosures, while also permitting impulse responses with more greatly varying properties.

By inverting the derivation in the appendix of [23], a modal frequency solution for the rigid walled rectangular-room boundary value problem can be obtained from Eq. 2. In [21], this solution was given for an n -D room in the form

$$p_{d_1 d_2 \dots d_n}(x_1, x_2, \dots, x_n) = C \prod_{i=1}^n \cos \left(\frac{d_i \pi x_i}{L_i} \right) \quad (6)$$

where d_i is an integer, n is the total number of spatial dimensions, L_i is the length of the room along the i th dimension, and C is a constant. What follows from here will be a time-domain solution to the n -D normal mode expansion using the image method.

3. N-DIMENSIONAL SPACE

3.1. n -D Acoustic Space

A room in n -D occupies a volume with units (distance) ^{n} . It is bound by a hypersurface with units (distance) ^{$n-1$} . The concept of 2-D walls is based on the presumption of a 3-D space. The concept of 2-D walls is thus replaced with the concept of ($n-1$)-D reflectors. As for time, it will be considered distinct from space and it will not be treated as a dimension. The discussion here will be limited to rectilinear room shapes, as other shapes in n -D space are beyond the scope of this paper.

Any dimension of space has both a positive and a negative direction. For an n -D room, the source and receiver, along any one dimension, are located between two reflectors. The total number of reflectors in an n -D room is thus equal to $2n$. A room in 4-D is depicted in Fig. 1.

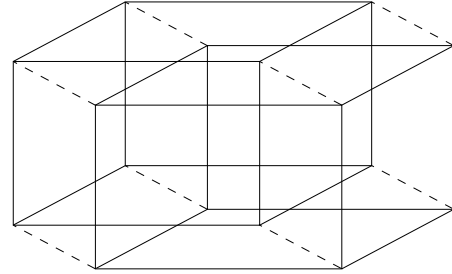


Figure 1: A 2-D parallel projection of a 4-D rectangular room.

3.1.1. Real Physical Systems for 1-D and 2-D

There are few, if any, tangible real-world systems analogous to an acoustic space with more than three dimensions. Acoustics tubes and plates, however, behave in a fashion similar to 1-D spaces and 2-D spaces, respectively. Waves in tubes are truly 1-D propagation of acoustic waves. Waves on plates propagate in 2-D, however, the propagation medium is metal and the waves are transverse rather than longitudinal. In [6] a comparative analysis was made between plates and rooms. Among the major differences is a phenomenon known as frequency dispersion. Frequency dispersion causes the propagation speed of a wave to vary with frequency. This occurs very significantly in plates, but not in rooms.

3.2. Reflection Coefficients

The constant A_q in Eqs. 1 and 3 includes a factor for the total reflection coefficient, which is itself the product of a set of reflection coefficients. Each reflection coefficient is given as $\beta = \pm \sqrt{1 - \alpha}$, where α is the absorption coefficient [34]. Classically the value of β is a positive number on the interval $[0, 1]$. Negative coefficients, however, have been studied as well [34] [35] [36]. In contrast to 3-D rooms, the reflection coefficients on 2-D plates are classically negative [31] [32]. This results in a reversal of the wave phase each time it is reflected by the plate boundary.

The value of a reflection coefficient depends on a number of factors. Because the existence of a higher dimensional room would require exotic forms of matter, the possible values for reflection coefficients can reasonably be presumed to include the interval $[-1, 1]$.

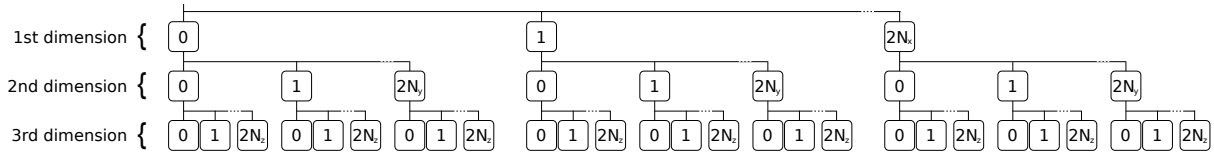


Figure 2: Iteration tree for calculation in 3-D. Dimension number increases top to bottom. Look-up table indices increase left to right. Image points are calculated for each leaf starting with the leftmost and moving to the right.

3.3. Energy Conservation and Pressure Amplitude

A sound source emits a finite amount of power. It is known that the distance attenuation of acoustic intensity is proportional to $1/r$ and $1/r^2$, for 2-D and 3-D, respectively [37]. Specifically in 3-D, acoustical intensity, or the power flux density, is $I_3 = P/4\pi r^2$, where the denominator is the area of a sphere with radius r . In 2-D, or equivalently, a cylindrical wave, the intensity is $I_2 = P/2\pi r^1$. Similarly, the intensity in a 1-D acoustic tube is $I_1 = P/2r^0$.

Integrating I_n for a source with power P over a closed Gaussian surface must yield the same value regardless of the problem's dimensionality. This results from the law of conservation of energy, and is shown as

$$\oint I(P)_m dS_m = \oint I(P)_n dS_n \quad (7)$$

where n and m are the number of dimensions. The expression for n -D power flux density can be written $I_n = P/S_{sn}$, where S_{sn} is the surface area of the n -D sphere. For a mention of several formulas for n -D geometry see Appendix A.

The calculation of an RIR requires a formula that relates sound pressure amplitude with distance. This formula should also be consistent with Eq. 7 and, hence, obey the law of energy conservation. Such a formula is given by

$$p(r)_n = \frac{A}{\sqrt{r^{n-1}}} \quad (8)$$

A derivation of Eq. 8 is provided in Appendix B.

4. COMPUTATIONAL PROCEDURE

For boxed-shaped rooms, the summation can be taken over each dimension. In [11], an algorithm using the formula

$$h(t) = \sum_{i=0}^{2N_x} \sum_{j=0}^{2N_y} \sum_{k=0}^{2N_z} p(t)_{ijk} \quad (9)$$

was used where $p(t)_{ijk}$ is the pressure impulse resulting from the ijk^{th} image in 3-D. In this case, i , j , and k are indices for look-up tables rather than indices for an image lattice. The summation operation is depicted graphically in Fig. 2 as a tree diagram. The algorithm has a reduced number of floating point operations compared to prior algorithms and thus has better performance. For this reason, a modified version of the algorithm was chosen for n -D calculations. The primary modification to the algorithm was to the summation procedure. For n -D, Eq. 9 can be written as

$$h(t) = \sum_{i_1=0}^{2N_1} \sum_{i_2=0}^{2N_2} \sum_{i_3=0}^{2N_3} \dots \sum_{i_n=0}^{2N_n} p(t)_{i_1 i_2 i_3 \dots i_n} \quad (10)$$

The tree diagram in Fig. 2 has a fractal structure that can similarly be extended to any number of dimensions. To perform calculations for a truly arbitrary number of dimensions, a scheme that recursively stepped into higher dimensions was used.

Square of the distance summations and reflection coefficient product operations were collected recursively on each function call. This resulted in fewer floating point operations than [11]. To account for distance losses, a relation based on Eq. 8 was used. RIRs for several different dimensions are plotted in Fig. 3.

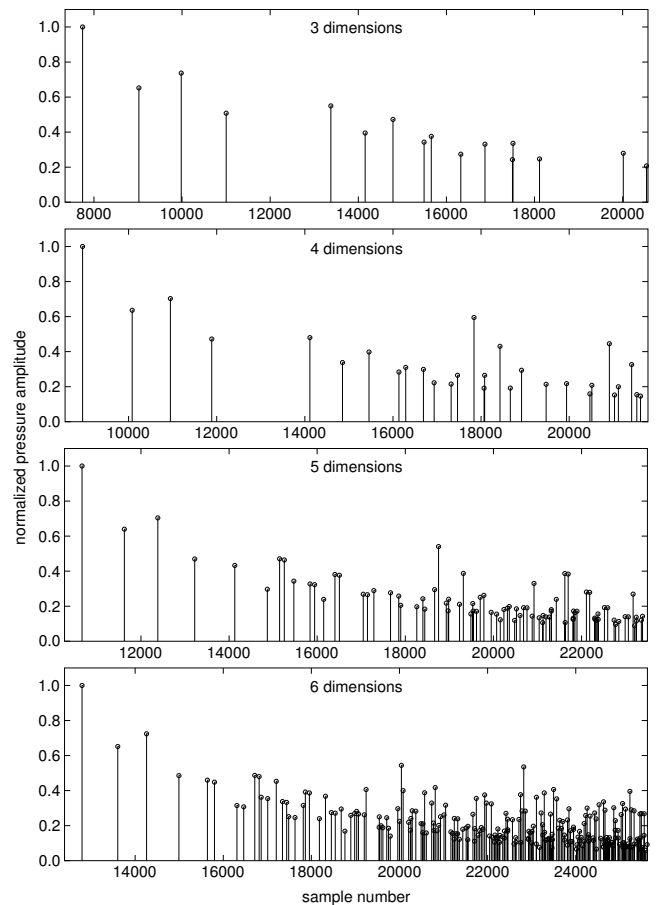


Figure 3: RIRs calculated for 3-D, 4-D, 5-D, and 6-D. Rooms measure approximately 10 meters in each dimension. RIRs are normalized and aligned to the first non-zero impulse.

5. ANALYTICAL IMPLICATIONS

The total number of echoes accounted for in an impulse response calculation of length t_{length} is given by the volume of an n -sphere of radius ct_{length} divided by the room volume. The result of this is given in by

$$E(t)_n = \frac{\pi^{\frac{n}{2}} c^n t^n}{\Gamma\left(\frac{n}{2} + 1\right) V_{rn}} \quad (11)$$

where Γ is the gamma function. The variable V_{rn} is the volume of the n -D room. The temporal echo density can be given by the time derivative of the total echo count, which leads to

$$\frac{dE}{dt}_n = \frac{2\pi^{\frac{n}{2}} c^n t^{n-1}}{\Gamma\left(\frac{n}{2}\right) V_{rn}} \quad (12)$$

On a 2-D plate, the echo density increases with t [6]. In a 3-D room, the echo density increases with t^2 . As is shown in Eq. 12, the echo density in an n -D space continues on with this pattern and increases with t^{n-1} . Plots for both Eqs. 11 and 12 are shown in Fig. 4.

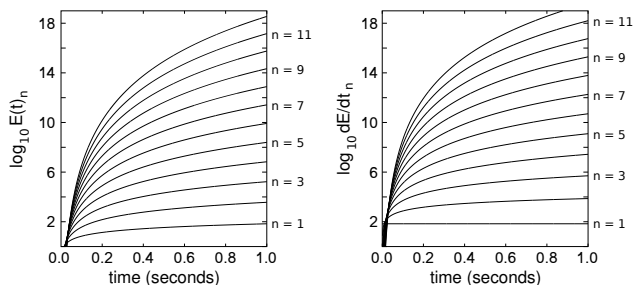


Figure 4: Plots for one to twelve spatial dimensions. left) total number of echoes, right) temporal echo density.

The literature describes various methods for calculating mixing time, many using different definitions [38] [39]. Generally, mixing time can be described as the transition from the early part of the response to the late part of the response. A commonly used definition for the point of transition is when the temporal echo density reaches some particular value. According to [2], this density is around 2000 - 4000 echoes / sec. Using 3000 echoes / sec as the transition point, the mixing time, t_{mix} , in n -D can be estimated as

$$t_{mix} = \left(3000 \frac{\Gamma\left(\frac{n}{2}\right) V_{rn}}{2\pi^{\frac{n}{2}} c^n} \right)^{\frac{1}{n-1}} \quad (13)$$

The mixing time is plotted for 1 to 45 dimensions in Fig. 5 on the left. It may be noted that a minimum occurs near $n = 8$. This occurs because dE/dt_n intersects dE/dt_m for $n \neq m$. This intersection is shown on the right in Fig. 5.

A curious effect that results from introducing additional dimensions to a given room configuration is that it increases the delay to existing impulses. Mathematically, this can be shown with an n -D extension of the Pythagorean theorem. It is illustrated in Fig. 3 where the delay time of the first impulse increases as the number of dimensions is increased. Here, the delay is observed as a shifted sample-time index. The delay can also be seen later in Fig. 6 as a change in distance to the nearest image point.

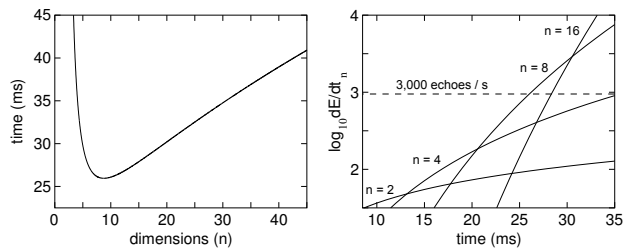


Figure 5: left) mixing times for rooms of n dimensions with $V_{rn} = 8^n$, right) temporal echo density for 2-D, 4-D, 8-D, and 16-D.

Because the computational costs have the potential to increase dramatically for higher dimensions, care must be taken in choosing input parameters. Table 1a shows, for a given dimension, the increase in the number of images as a factor when the time-length of the output RIR is increased by a factor of 2.

Table 1: a) Increase in sphere volume when the time-length of the impulse response is increased by a factor of 2. b) Required room volume V_{rm} when $E(t)_m = E(t)_n$ and $r = 68.6$.

| (a) | | (b) | |
|-----|------------------------|-----|-----------------|
| n | $V(2t)_{sn}/V(t)_{sn}$ | m | V_{rm}/V_{r3} |
| 1 | 2 | 1 | 1.01 e -04 |
| 2 | 4 | 2 | 1.09 e -02 |
| 3 | 8 | 3 | 1.00 e +00 |
| 4 | 16 | 4 | 8.08 e +01 |
| 5 | 32 | 5 | 5.91 e +03 |
| 6 | 64 | 6 | 3.98 e +05 |
| 7 | 128 | 7 | 2.50 e +07 |
| 8 | 256 | 8 | 1.47 e +09 |
| 9 | 512 | 9 | 8.21 e +10 |
| 10 | 1024 | 10 | 4.35 e +12 |

The higher computational costs of higher dimensional RIRs can be offset by using rooms with larger volumes. This is true presuming that the total time-length of the output RIR is held fixed. Computational costs for higher dimensional rooms will be similar to that of lower dimensional rooms if the total number of image points considered in each calculation is also similar. To estimate an m -D room volume that will produce an RIR with a similar number of image points as a given n -D room, the number of echoes from Eq. 11 can be set so that $E(t)_m = E(t)_n$. Solving for V_{rm} results in

$$V_{rm} = \frac{\pi^{\frac{m}{2}} r^m \Gamma\left(\frac{n}{2} + 1\right)}{\pi^{\frac{n}{2}} r^n \Gamma\left(\frac{m}{2} + 1\right)} V_{rn} \quad (14)$$

The relative increase in volume resulting from Eq. 14 is shown in Table 1b for $n = 3$, $r = 68.6$ and various values of m .

If the total number of images can not be reduced, there are still other approaches that may prove useful for modeling n -D systems. The tail portion of RIRs have a strong noise-like behavior. Modeling this behavior has been shown to reduce computational costs for 3-D systems [40] and it is likely that this type of approach can also be extended to n -D.

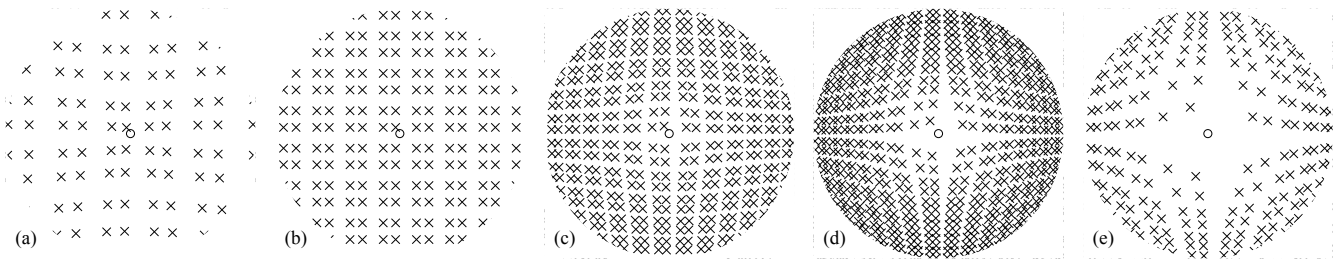


Figure 6: Diagrams of 2-D virtual source lattices radially transposed. The resultant temporal echo density profiles correspond to: a) 1.7 dimensions, b) 2.0 dimensions (original), c) 2.5 dimensions, d) 3.3 dimensions, e) 4.2 dimensions.

6. FRACTIONAL DIMENSIONS AND LATTICE TRANSPOSITION

It is possible to transpose a lattice of virtual sources from an n -D temporal echo density to an m -D temporal echo density. This can shape the pseudorandom behavior of the echoes and result in an IR with properties of an m -dimensional lattice. In this case, m can be any positive number including non-integers. The approach that follows is to generate a lattice of virtual sources and to then transpose them radially around the receiver.

Given an n -D lattice, each virtual source has a relative radial location with respect to the receiver. This radius is given by Δr_n . To obtain a transposition function, assume that $E_n = E_m$, where E is given by Eq. 11 and m is the desired dimensionality. Next, within the formulas for E_n and E_m , replace the variables $c^n t^n$ and $c^m t^m$ with the equivalent Δr_n^n and Δr_m^m , respectively. This results in

$$\frac{\pi^{\frac{n}{2}} \Delta r_n^n}{\Gamma(\frac{n}{2} + 1) V_{rn}} = \frac{\pi^{\frac{m}{2}} \Delta r_m^m}{\Gamma(\frac{m}{2} + 1) V_{rm}} \quad (15)$$

Solving Eq. 15 for Δr_m results in the transposition function

$$\Delta r_m = \eta \Delta r_n^{\frac{n}{m}} \quad (16)$$

where Δr_m is the new radius and η is a constant given by

$$\eta = \left(\frac{\pi^{\frac{n}{2}} \Gamma(\frac{m}{2} + 1) V_{rm}}{\pi^{\frac{m}{2}} \Gamma(\frac{n}{2} + 1) V_{rn}} \right)^{\frac{1}{m}} \quad (17)$$

Radially transposed image lattices, along with the original 2-D lattice, are shown in Fig. 6.

7. RESULTS

7.1. Computational Complexity

The fast image method is demonstrably faster than the Allen and Berkley algorithm [40][11]. There is limited discussion in the literature, however, on the theoretical basis for this. There has also never before been an extension to n -D.

7.1.1. Mathematical and Algorithmic Theory

Computation time in existing algorithms [23][11] is dependent on many factors. Much of the computational costs result from calculating the distances to the virtual sources. Distance calculations for sources outside the "sphere of interest" are unnecessary and can be

omitted [11]. This omission leads to a theoretical speedup factor for the distance calculations that is given as the ratio of the volume of an n -cube over the volume of an inscribed n -sphere. This is given as

$$s_{nd} = \frac{2^n \Gamma(\frac{n}{2} + 1)}{\pi^{\frac{n}{2}}} \quad (18)$$

Some values of s_{nd} are given in Table 2. When the number of dimensions is $n = 20$, the number of distance calculations is reduced by a factor of 4.1×10^7 , and thus the total computation time ought to be dramatically reduced.

Table 2: Reduction factor for the number of distance calculations in n -D space.

| n | s_{nd} |
|-----|--------------|
| 1 | 1.0000 e +00 |
| 2 | 1.2732 e +00 |
| 3 | 1.9099 e +00 |
| 4 | 3.2423 e +00 |
| 5 | 6.0793 e +00 |
| 6 | 1.2385 e +01 |
| 7 | 2.7091 e +01 |
| 8 | 6.3074 e +01 |
| 9 | 1.5522 e +02 |
| 10 | 4.0154 e +02 |
| 11 | 1.0870 e +03 |
| 12 | 3.0676 e +03 |
| 13 | 8.9960 e +03 |
| 14 | 2.7340 e +04 |
| 15 | 8.5905 e +04 |
| 16 | 2.7848 e +05 |
| 17 | 9.2971 e +05 |
| 18 | 3.1912 e +06 |
| 19 | 1.1246 e +07 |
| 20 | 4.0632 e +07 |

The Allen and Berkley algorithm calculates the total reflection coefficient as

$$\beta_{total} = \beta_{x_{1,1}}^{|i_1 - u_1|} \beta_{x_{1,2}}^{|i_1|} \beta_{x_{2,1}}^{|i_2 - u_2|} \beta_{x_{2,2}}^{|i_2|} \beta_{x_{3,1}}^{|i_3 - u_3|} \beta_{x_{3,2}}^{|i_3|} \dots \beta_{x_{n,1}}^{|i_n - u_n|} \beta_{x_{n,2}}^{|i_n|} \quad (19)$$

where the i 's and the u 's are indices corresponding to the room index. This requires $2n$ multiplies, $2n$ exponentiations, and n subtractions. Each exponentiation can be calculated by either a product summation or by using the identity

$$\beta_x^{|i|} = e^{|i| \ln \beta} \quad (20)$$

which is classically expressed as a series expansion.

In contrast, the algorithm in [11], calculates the total reflection coefficient as

$$\beta_{total} = \beta_{x_1, i_1} \beta_{x_2, i_2} \beta_{x_3, i_3} \dots \beta_{x_n, i_n} \quad (21)$$

where the value of each $\beta_{x,i}$ is taken from a look-up table. This requires n multiplies, 0 exponentiations, and 0 subtractions. While some computation time is needed to produce the look-up tables, it is small and only becomes significant when the calculation is limited to low order reflections.

Computation time is also required when calculating the pressure amplitude distance relation given in Eq. 8. The denominator has the term r^{n-1} . Because $n - 1$ is always an integer, the value of the exponentiation can be calculated by either a series of multiplies or as a series expansion of Eq. 20. By using the former, total computation time was reduced by around one half for calculations in 6-D.

7.1.2. Benchmarks

Both the Allen and Berkley algorithm and the fast image method were programmed for a fixed number of dimensions. This effort was continued until both algorithms had been programmed for all dimensions from one up through eight. Each of the 16 algorithms ran within a small separate standalone executable. Benchmarks were performed on a Linux system, and the `time` command was used to measure program run-time. Each program was set to loop its respective algorithm a fixed number of times so that the total run-time was at least one second. The average algorithm run-time was then calculated and used to find the speedup factor.

When considering program run-time, the time-length of the RIR filter should be considered relative to the room volume. In fact, time-length and room volume can be used to accurately estimate the total number of image points, and this will correlate very well with total execution time. Time-length is an important property of an RIR, and for this reason, benchmarks were made with time-length as an input variable. Because different time-lengths cause the number of mathematical operations to vary somewhat, benchmarks were performed for two time-lengths: t_1 and $2t_1$.

The results of the tests are listed in Table 3. The speedup factor for time-length t_1 starts at 1.5 for 1-D and steadily increases to 316.0 for 8-D. For time-length $2t_1$ the results were similar with a factor of 1.6 for 1-D and 210.0 for 8-D. The speedup factors obtained for 3-D were similar to those obtained in [11] and [40].

Both the number of image points and the computation time increased greatly with the number of dimensions. For the 8-D Allen and Berkley algorithm with time-length $2t_1$, the algorithm run-time was nearly three hours. It's expected that benchmarks in dimensions higher than eight would consume an unreasonable amount of time.

In theory, the outputs from the two algorithms are identical. In practice, there is a slight difference due to the way that each implementation produces floating-point round-off error. The difference, however, is small and the two outputs can still be validated against one another.

Table 3: Speedup factor s_n for RIRs of length t_1 and $2t_1$.

| n | t_1 | | $2t_1$ | |
|-----|-------|--------------|--------|--------------|
| | s_n | image points | s_n | image points |
| 1 | 1.5 | 7 | 1.6 | 17 |
| 2 | 1.8 | 57 | 2.0 | 236 |
| 3 | 6.1 | 311 | 7.1 | 2,725 |
| 4 | 23.6 | 1,618 | 13.5 | 28,033 |
| 5 | 70.2 | 7,929 | 30.8 | 262,155 |
| 6 | 133.0 | 35,660 | 64.3 | 2,262,971 |
| 7 | 230.6 | 147,327 | 147.7 | 18,206,694 |
| 8 | 316.0 | 562,993 | 210.0 | 137,616,917 |

7.2. Evaluation

Using the methods laid out in this paper, impulse responses of rooms from one to twelve spatial dimensions have been calculated. Calculations in dimensions higher than twelve are also possible.

By transposing the locations of virtual sources, n -D lattices have been forced to produce the same temporal echo densities as both higher and lower dimensional lattices. Image lattices have also been transposed to fractional dimensions, and the range of this extends below 1-D.

Calculated RIRs have been convolved with audio signals to perform n -D room simulations. All simulations sounded similar to reverberation. Simulations in 1-D produced delay type effects while simulations that had been scaled to dimensions near 1-D produced exotic delay type effects. In 2-D, they produced a reverberation effect and the RIR had plate-like properties. It is interesting to note that calculations in the frequency domain could model frequency dispersion and this would result in RIRs with even more plate-like properties. In 3-D, RIRs produced reverberant-like effects. In dimensions above three, the effects were also reverberant like. It was noted that decay times seemed to drop off more abruptly, although a rigorous numerical analysis would be more informative.

8. CONCLUSIONS

The image method has been generalized to n -D. Acoustic spaces up to 12-D have been simulated, and the behavior of fractional dimensions has been modeled. Strong similarities between delay, plate, and room reverberation have been illustrated.

Computation time increases significantly with each additional dimension. Use of the fast image method dramatically reduced the number of computations. Its use became critical for higher dimensional calculations where computation time became an issue.

9. REFERENCES

- [1] P. Huang, J.S. Abel, "Aspects of reverberation echo density," in *Audio Eng. Soc. Convention (123)*, New York, United States, Oct. 5-8, 2007, p. 7163.
- [2] J.S. Abel, P. Huang, "A simple, robust measure of reverberation echo density," in *Audio Eng. Soc. Convention (121)*, San Francisco, United States, Oct. 5-8, 2006, p. 6985.

- [3] P. Huang, J.S. Abel, H. Terasawa, J. Berger, "Reverberation echo density psychoacoustics," in *Audio Eng. Soc. Convention (125)*, San Francisco, United States, Oct. 2-5, 2008, p. 7583.
- [4] J. Parker, S. Bilbao, "Spring reverberation: A physical perspective," in *Proc. Digital Audio Effects (DAFx-09)*, Como, Italy, Sept. 1-4, 2009.
- [5] S. Bilbao, J. Parker, "A virtual model of spring reverberation," *IEEE Trans. Audio, Speech, Language Processing*, vol. 18, no. 4, 2010.
- [6] K. Arcas, A. Chaigne, "On the quality of plate reverberation," *Appl. Acoust.*, vol. 71, no. 2, pp. 147–156, 2010.
- [7] S. Bilbao, L. Savioja, J.O. Smith III, "Parameterized finite difference schemes for plates: Stability, the reduction of directional dispersion and frequency warping," *IEEE Trans. Audio, Speech, Language Processing*, vol. 15, no. 4, 2007.
- [8] F. Avanzini, *Algorithms for Sound and Music Computing*, chapter 4, Dec 2008.
- [9] C. Borß, "A VST reverberation effect plugin based on synthetic room impulse responses," in *Proc. of the Int. Conf. on Digital Audio Effects (DAFx-09)*, Como, Italy, Sept. 1-4, 2009.
- [10] L. Savioja, "Real-time 3D finite-difference time-domain simulation of low- and mid-frequency room acoustics," in *Proc. of the Int. Conf. on Digital Audio Effects (DAFx-10)*, Graz, Austria, Sept. 6-10, 2010.
- [11] S.G. McGovern, "Fast image method for impulse response calculations of box-shaped rooms," *Appl. Acoust.*, vol. 70, no. 1, pp. 182–189, 2009.
- [12] A. Kulowski, "Algorithmic representation of the ray tracing technique," *Appl. Acoust.*, vol. 18, no. 6, pp. 449–469, 1985.
- [13] S. Laine, S. Siltanen, T. Lokki, L. Savioja, "Accelerated beam tracing algorithm," *Appl. Acoust.*, vol. 70, no. 1, pp. 172–181, 2009.
- [14] Z.Y. Huang, W.K. Jiang, "An effective method calculating acoustic Green's function for closed rectangular cavity using the Ewald's summation technique," *Acta Acust. Acust.*, vol. 93, no. 5, pp. 853–856, 2007.
- [15] R. Duraiswami, D.N. Zotkin, N.A. Gumerov, "Fast evaluation of the room transfer function using multipole expansion," *IEEE Trans. Audio, Speech, Language Processing*, vol. 15, no. 2, 2007.
- [16] N. Tsingos, I. Carlbom, G. Elko, R. Kubli, T. Funkhouser, "Validating acoustical simulations in the Bell Labs Box," *IEEE Comp. Graph. and Apps.*, vol. 22, no. 4, pp. 28–37, 2002.
- [17] H. Penttinen, M. Karjalainen, T. Paatero, H. Järveläinen, "New techniques to model reverberant instrument body responses," in *Proc. Intl. Computer Music Conf. (ICMC-01)*, La Habana, Cuba, Sept. 18-22, 2001.
- [18] M. Karjalainen, J.O. Smith III, "Body modeling techniques for string instrument synthesis," in *Proc. Intl. Computer Music Conf. (ICMC-96)*, Hong Kong, 1996.
- [19] C.B. Maxwell, "Real-time reverb simulation for arbitrary object shapes," in *Proc. Digital Audio Effects (DAFx-07)*, Bordeaux, France, Sept. 10-15, 2007.
- [20] L. Savioja, M. Karjalainen, T. Takala, "DSP formulation of a finite difference method for room acoustics simulation," in *Proc. IEEE Nordic Signal Processing Symp. (NORSIG'96)*, Espoo, Finland, Sept. 1996, pp. 455–458.
- [21] A. Kelloniemi, V. Välimäki, P. Huang, L. Savioja, "Artificial reverberation using a hyper-dimensional FDTD mesh," in *Proc. European Signal Processing Conf. (EUSIPCO-05)*, Sept. 2005.
- [22] A. Kelloniemi, V. Välimäki, P. Huang, L. Savioja, "Hyper-dimensional digital waveguide mesh for reverberation modeling," in *Proc. Digital Audio Effects (DAFx-07)*, Bordeaux, France, Sept. 10-15, 2007.
- [23] J.B. Allen, D.A. Berkley, "Image method for efficiently simulating small-room acoustics," *J. Acoust. Soc. Am.*, vol. 65, no. 4, pp. 943–950, 1979.
- [24] D.T. Murphy, D.M. Howard, "Modelling and directionally encoding the acoustics of a room," *Electronics Letters*, vol. 34, no. 9, pp. 864–865, 1998.
- [25] D.T. Murphy, D.M. Howard, "2-D digital waveguide mesh topologies in room acoustics modelling," in *Proc. Digital Audio Effects (DAFx-00)*, Verona, Italy, Dec. 7-9, 2000.
- [26] D.T. Murphy, A. Kelloniemi, J. Mullen, S. Shelley, "Acoustic modeling using the digital waveguide mesh," *IEEE Signal Processing Magazine*, vol. 24, no. 2, pp. 55–66, 2007.
- [27] J. Moorer, "About this reverberation business," *Comp. Music Journal*, vol. 3, no. 2, pp. 13–28, 1979.
- [28] M. Foco, P. Polotti, A. Sarti, S. Tubaro, "Sound spatialization based on fast beam tracing in the dual space," in *Proc. Digital Audio Effects (DAFx-03)*, London, UK, Sept. 8-11, 2003.
- [29] F. Antonacci, M. Foco, A. Sarti, S. Tubaro, "Fast tracing of acoustic beams and paths through visibility lookup," *IEEE Trans. Audio, Speech, Language Processing*, vol. 16, no. 4, 2008.
- [30] J. Brunskog, "Image solution for clamped finite beams," *J. Sound Vib.*, vol. 287, no. 4-5, pp. 1057–1064, 2005.
- [31] R. Gunda, S.M. Vijayakar, R. Singh, "Method of images for the harmonic response of beams and rectangular plates," *J. Sound Vib.*, vol. 185, no. 5, pp. 791–808, 1995.
- [32] J. Cuenca, F. Gautier, L. Simon, "The image source method for calculating the vibrations of simply supported convex polygonal plates," *J. Sound Vib.*, vol. 322, no. 4-5, pp. 1048–1069, 2009.
- [33] G. Arfken, H. Weber, *Mathematical Methods for Physicists*, p. 911, Academic Press, San Diego, CA, USA, 2001.
- [34] E.A. Lehmann, A.M. Johansson, "Prediction of energy decay in room impulse responses simulated with an image-source model," *J. Acoust. Soc. Am.*, vol. 124, no. 1, pp. 269–277, 2008.
- [35] J. António, L. Godinho, A. Tadeu, "Reverberation times obtained using a numerical model versus those given by simplified formulas and measurements," *Acta Acust. Acust.*, vol. 88, no. 2, pp. 252–261, 2002.
- [36] M. Gorzel, G. Kearney, F. Boland, H. Rice, "Virtual acoustic recording: An interactive approach," in *Proc. of the Int. Conf. on Digital Audio Effects (DAFx-10)*, Graz, Austria, Sept. 6-10, 2010.

- [37] A. Kelloniemi, V. Välimäki, L. Savioja, “Simulation of room acoustics using 2-D digital waveguide meshes,” in *Intl. Conf. Acoust. Speech and Signal Processing (ICASSP-06)*, Toulouse, France, May 14-19, 2006.
- [38] K. Meesawat, D. Hammershøi, “An investigation on the transition from early reflections to a reverberation tail in a BRIR,” in *Proc. of the Int. Conf. on Auditory Display (ICAD02)*, Kyoto, Japan, July 2-5, 2002.
- [39] A. Lindau, L. Kosanke, S. Weinzierl, “Perceptual evaluation of physical predictors of the mixing time in binaural room impulse responses,” in *Audio Eng. Soc. Convention (128)*, London, United Kingdom, May 22-25, 2010, p. 8089.
- [40] E.A. Lehmann, A.M. Johansson, “Diffuse reverberation model for efficient image-source simulation of room impulse responses,” *IEEE Trans. Audio, Speech, Language Processing*, vol. 18, no. 6, 2010.
- [41] D. Halliday, R. Resnick, J. Walker, *Fundamentals of Physics*, chapter 18, John Wiley & Sons, Inc, New York, USA, fifth edition, 1997.

A. APPENDIX: N-D GEOMETRIC FORMULAS

The volume of an n -D room is given by

$$V_{rn} = \prod_{i=1}^n L_i \quad (22)$$

The volume of an n -sphere is given by

$$V_{sn} = \frac{\pi^{\frac{n}{2}} r^n}{\Gamma\left(\frac{n}{2} + 1\right)} \quad (23)$$

where r is the radius of the sphere and Γ is the gamma function. The surface area is the derivative of the volume. Using the gamma function identity

$$\frac{2}{\Gamma\left(\frac{n}{2}\right)} = \frac{n}{\Gamma\left(\frac{n}{2} + 1\right)} \quad (24)$$

the surface area of an n -sphere is given by

$$S_{sn} = \frac{2\pi^{\frac{n}{2}} r^{n-1}}{\Gamma\left(\frac{n}{2}\right)} \quad (25)$$

B. APPENDIX: DERIVATION OF N-D PRESSURE DISTANCE RELATION

There are a number of acoustics-related relations that can be found in general physics texts [41]. The following derivation will be based heavily around this.

The acoustic pressure amplitude is given by

$$p = v\rho\omega s \quad (26)$$

where v is the propagation speed of the wave, ρ is the mass density, ω is the angular frequency, and s is the displacement amplitude. The acoustical kinetic energy contained in an infinitesimal element of air is given by

$$dK = \frac{1}{2} dm v_s^2 \quad (27)$$

where v_s is the velocity of the oscillating air mass element dm . For a spherical wave traveling radially outward, v_s is given by

$$v_s = -\omega s \sin(kr - \omega t) \quad (28)$$

The mass of the air element is given by multiplying density ρ by the volume element. For an n -D spherical wave, the volume element is given by the product of the surface area of an n -sphere and an infinitesimal shell thickness dr . For the mass element, this results in

$$dm_n = \rho \frac{2\pi^{\frac{n}{2}} r^{n-1}}{\Gamma\left(\frac{n}{2}\right)} dr \quad (29)$$

Substituting Eqs. 28 and 29 into Eq. 27 results in

$$dK = \frac{1}{2} \left(\rho \frac{2\pi^{\frac{n}{2}} r^{n-1}}{\Gamma\left(\frac{n}{2}\right)} dr \right) \omega^2 s^2 \sin^2(kr - \omega t) \quad (30)$$

The rate of flow of kinetic energy can be shown to be

$$\frac{dK}{dt} = \rho \frac{\pi^{\frac{n}{2}} r^{n-1}}{\Gamma\left(\frac{n}{2}\right)} v \omega^2 s^2 \sin^2(kr - \omega t) \quad (31)$$

where the propagation speed v is equal to dr/dt . It follows that the time average of the kinetic energy flow rate is given by

$$\overline{\left(\frac{dK}{dt}\right)} = \frac{1}{2} \rho \frac{\pi^{\frac{n}{2}} r^{n-1}}{\Gamma\left(\frac{n}{2}\right)} v \omega^2 s^2 \quad (32)$$

where the time average of $\sin^2(kr - \omega t) = \frac{1}{2}$. The power transmitted is equal to the sum of the rates of both the kinetic energy and the potential energy. This is equivalent to two times the average kinetic energy.

$$P = \overline{\left(\frac{dK}{dt}\right)} + \overline{\left(\frac{dU}{dt}\right)} = 2 \overline{\left(\frac{dK}{dt}\right)} \quad (33)$$

Substituting Eq. 32 into 33 and simplifying results in

$$P = \rho \frac{\pi^{\frac{n}{2}} r^{n-1}}{\Gamma\left(\frac{n}{2}\right)} v \omega^2 s^2 \quad (34)$$

Solving for s results in an expression for the n -D particle displacement.

$$s = \sqrt{\frac{P \Gamma\left(\frac{n}{2}\right)}{\rho v \omega^2 \pi^{\frac{n}{2}} r^{n-1}}} \quad (35)$$

Substituting Eq. 35 into Eq. 26 gives

$$p = (v\rho\omega) \sqrt{\frac{P \Gamma\left(\frac{n}{2}\right)}{\rho v \omega^2 \pi^{\frac{n}{2}} r^{n-1}}} = \sqrt{\frac{v\rho P \Gamma\left(\frac{n}{2}\right)}{\pi^{\frac{n}{2}} r^{n-1}}} \quad (36)$$

Finally, setting

$$A = \sqrt{\frac{v\rho P \Gamma\left(\frac{n}{2}\right)}{\pi^{\frac{n}{2}}}} \quad (37)$$

Eq. 36 can be rewritten as

$$p(r)_n = \frac{A}{\sqrt{r^{n-1}}} \quad (38)$$

In Eqs. 1 and 3, the constant A_q is assumed to include an additional factor for the total reflection coefficient.